

GRAVITATIONAL WAVE OBSERVATIONS MAY CONSTRAIN GAMMA-RAY BURST MODELS: THE CASE OF GW 150914 - GBM

P. VERES¹, R. D. PREECE², A. GOLDSTEIN^{3,4}, P. MÉSZÁROS⁵, E. BURNS⁶ AND V. CONNAUGHTON³

¹ CSPAR, University of Alabama in Huntsville, 320 Sparkman Dr., Huntsville, AL 35805, USA

²Dept. of Space Science, University of Alabama in Huntsville, 320 Sparkman Dr., Huntsville, AL 35805, USA

³Universities Space Research Association, 320 Sparkman Dr. Huntsville, AL 35806, USA

⁴Astrophysics Office, ZP12, NASA/Marshall Space Flight Center, Huntsville, AL 35812, USA

⁵Dept. of Astronomy and Astrophysics, Pennsylvania State University, 525 Davey Laboratory, University Park, PA 16802, USA

⁶Physics Dept., University of Alabama in Huntsville, 320 Sparkman Dr., Huntsville, AL 35805, USA

ABSTRACT

The possible short gamma-ray burst (GRB) observed by *Fermi*/GBM in coincidence with the first gravitational wave (GW) detection, offers new ways to test GRB prompt emission models. Gravitational wave observations provide previously inaccessible physical parameters for the black hole central engine such as its horizon radius and rotation parameter. Using a minimum jet launching radius from the Advanced LIGO measurement of GW 150914, we calculate photospheric and internal shock models and find that they are marginally inconsistent with the GBM data, but cannot be definitely ruled out. Dissipative photosphere models, however have no problem explaining the observations. Based on the peak energy and the observed flux, we find that the external shock model gives a natural explanation, suggesting a low interstellar density ($\sim 10^{-3} \text{ cm}^{-3}$) and a high Lorentz factor (~ 2000). We only speculate on the exact nature of the system producing the gamma-rays, and study the parameter space of a generic Blandford Znajek model. If future joint observations confirm the GW-short GRB association we can provide similar but more detailed tests for prompt emission models.

1. INTRODUCTION

With the first detection of GWs we entered a new era in astrophysics (Abbott et al. 2016a). Electromagnetic counterparts are crucial for establishing the astrophysical context for the GWs and also for a more accurate localization to aid subsequent follow-up (Connaughton et al. 2015). GRB progenitors (see Meszaros & Rees 2014; Kumar & Zhang 2015, for reviews) have been leading candidates for sources of GWs (Kobayashi & Mészáros 2003; Corsi & Mészáros 2009). The most widely considered GW sources are compact binary mergers with components stemming from a combination of neutron stars (NS) or black holes (BH). Other than BH-BH mergers, substantial radiation is expected to accompany the GW signal, and indeed, the leading candidate for short-hard GRBs are merging neutron stars (Paczynski 1986; Eichler et al. 1989). The GW 150914 event is best explained by the merger of two $\sim 30 M_{\odot}$ black holes. *Fermi*/GBM detected a tantalizing counterpart, GW 150914-GBM (Connaughton et al. 2016), consistent with a weak short GRB, broadly consistent

with the GW location and temporally coincident with the GW signal (offset of $\Delta t_{\gamma\text{-GW}} \approx t_{\text{GRB}} - t_{\text{GW}} = 0.4 \text{ s}$). We note however that while Advanced LIGO and GBM locations are consistent, they both span a significant portion of the sky (~ 600 square degrees for Advanced LIGO at 90% confidence level and ~ 3000 square degrees for GBM at 68% confidence level). This observation potentially marks the beginning of the multi-messenger astrophysics.

In this paper we assume the weak GBM burst is a GRB (we refer to it as GW 150914-GBM) associated with GW 150914 and investigate its implications for the physical parameters of the system and for its surroundings. This joint electromagnetic (EM), GW observation was already addressed in a significant number of early studies covering aspects of EM energy extraction from a binary BH system and its surroundings (Li et al. 2016; Loeb 2016; Perna et al. 2016; Frascchetti 2016; Yamazaki et al. 2016; Zhang 2016).

INTEGRAL ACS observations (Savchenko et al. 2016) set a constraining upper limit in terms of the source fluence in the ACS energy range (above $\sim 75 \text{ keV}$). The uncertainties on the GBM spectral parameters and on the direction of the possible source, however, weaken any

tension between the two measurements (for details, see Section 3.3 of [Connaughton et al. 2016](#)). Nonetheless, we emphasize that the association between the GBM event and GW 150914 might have occurred by chance. However, because the false alarm probability of the two events being associated is $P=2.2 \times 10^{-3}$ ([Connaughton et al. 2016](#)), we will *assume* a common origin and venture to discuss the implications for the GRB emission models.

There has been considerable uncertainty in the GRB prompt emission model parameters, such as the compact object mass and rotation rate. For the first time however we can use realistic input parameters for modeling the BH central engine, because the gravitational wave observations yield these parameters to a precision that was previously unavailable. We calculate, to the extent that the gamma-ray observations allow, the constraints on the usual GRB models that can be placed.

Jets and black hole central engines are thought to be ubiquitous in GRBs. Energy released from the central engine becomes collimated either by magnetic stresses or the ram pressure of a progenitor star. The initial dynamics of the jet are determined by the launching radius, the size of the base of the jet, where the Lorentz factor of the matter, which eventually produces the GRB, is around unity. In other words the launching radius (R_0) is the characteristic size of the volume in which energy is deposited. It is beyond this radius that the jet starts to accelerate.

Current methods of determining the launching radius rely on the blackbody components in the GRB spectrum ([Pe’er et al. 2007](#)). [Larsson et al. \(2015\)](#) found the launching radius for GRB 101219B is approximately 10 times the horizon radius. This suggests the launching radius is defined by the scale of the BH central engine rather than larger scales ($\gtrsim 10^9$ cm) such as the progenitor star (e.g. in the case of reconfinement shocks, [Nalewajko \(2012\)](#)). Even considering substantial progress in jet modeling, the launching radius is one of the least well constrained physical parameters of the fireball model. The gravitational wave observations can determine the parameters of the resulting black hole and give a strict lower limit on the launching radius.

In the next section we list the observational properties of the GW and γ -ray event. In Section 3, we briefly speculate on the parameters of the gamma-ray emitting system. In Section 4, we mention GRB radiation models in the context of this source. Finally, we discuss our results in Section 5. For quantity Q , we use the $Q_x = Q/10^x$ scaling notation in cgs units and the physical constants have the usual meanings.

2. OBSERVATIONS

2.1. Gravitational waves

The energy released in GW 150914, $E_{\text{GW}} \approx 3M_{\odot}c^2 \approx 5.4 \times 10^{54}$ erg is comparable to the isotropic equivalent energy release of very bright GRBs. The final mass of the merged BH is $M_{\text{BH}} = 62 \pm 4M_{\odot}$ and its rotation parameter is $a = 0.67_{-0.07}^{+0.05}$ ([Abbott et al. 2016a](#)). The gravitational radius of a 62 solar mass BH is $R_G = GM_{\text{BH}}/c^2 = 9.2 \times 10^6$ cm, the horizon radius is $R_H = (1 + \sqrt{1 - a^2})R_G = 1.6 \times 10^7$ cm.

The innermost stable orbit which we later associate with the launching radius of the jet, is at $R_0 \approx f_1(a)R_G = 3.2 \times 10^7$ cm. $f_1(a = 0.67) = 3.5$, where $f_1(a) = 2 - a + 2(1 - a)^{1/2}$.

GRB models usually invoke jets emitted along the rotation axis of their progenitor BH. Due to Doppler boosting we can further assume our viewing angle is within the opening angle of the jet, otherwise the EM emission would be highly suppressed (essentially undetectable). The most favorable configuration for both GW detection and jetted emission is in case we view the binary system, perpendicular to the rotation plane. The GW signal does not have a strong dependence on the viewing angle. All things being equal, the difference in GW signal-to-noise from a face-on to an edge-on configuration is a factor of $\sqrt{8} \approx 2.8$. Due to a known degeneracy between the inclination angle and distance ([Cutler & Flanagan 1994](#); [Abbott et al. 2016b](#)), basically all the inclination angles are allowed by GW data. The observed γ -rays however suggest that we see the system close to face-on.

2.2. Gamma-rays

GBM detected a weak source with duration of $T_{\gamma} \approx 1$ s which, at the time of the GW trigger was in an unfavorable position for the GBM detectors. Careful analysis however reveals a source with parameters consistent with a short GRB ([Connaughton et al. 2016](#)).

GBM count spectra were deconvolved with detector response matrices for multiple positions within the joint GBM/LIGO localization region. The resulting fit is mostly consistent with a hard power law, with photon index $\alpha_{\text{PL}} = -1.40_{-0.24}^{+0.18}$. This power law index is consistent with other weak short GRBs that have been detected by GBM that can only be fit by a power law due to their low flux. The median (mean) value for the PL index for all weak GBM short GRBs is -1.36 (-1.40). The luminosity in the 1 keV to 10 MeV range, which is a good approximation for the bolometric luminosity, is $L_{\text{obs}} \approx 2.3 \times 10^{49}$ erg s $^{-1}$.

Hints for a possible cutoff energy come from one of the positions on the initial localization annulus, where it was possible to constrain a physically more realistic, Comp-

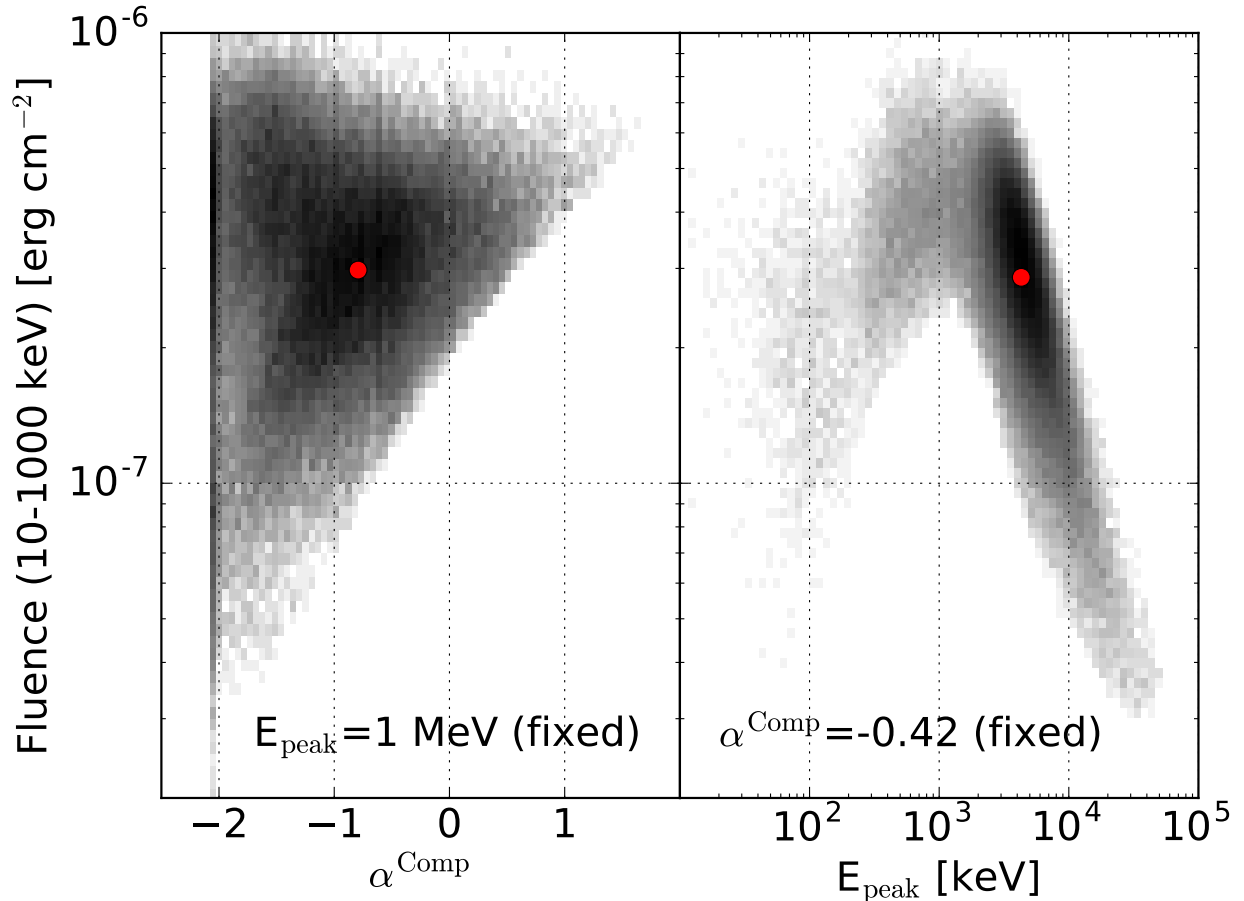


Figure 1. Spectral parameters using the Comptonized model. In the left panel we fix the peak energy to 1 MeV and display the distribution of the power law index versus fluence. In the right panel we plot the distribution of the peak energy similarly against fluence, when the power law index is fixed at the average for short GRBs, $\alpha^{\text{Comp}} = -0.42$. Red dots mark the peak of the histograms.

tonized spectrum (power law with exponential cutoff):¹

$$\frac{dN_{\text{ph}}}{dE} = A \left(\frac{E}{100 \text{ keV}} \right)^{\alpha^{\text{Comp}}} \exp \left(-\frac{E(\alpha + 2)}{E_{\text{pk}}^{\text{Comp}}} \right). \quad (1)$$

Short GRBs are typically well fit using this model, with high peak energies and a steep spectrum above the peak energy. The assumed source position however is not compatible with the relative count rates measured in the 14 GBM detectors, and is excluded at the 90% confidence level by the *joint* GBM-LIGO localization.

The event is too weak to confidently constrain more than two spectral parameters. Since the best fitting power law spectrum is ultimately unphysical because it implies infinite amount of liberated energy, we carry out

Monte Carlo simulations to evaluate the ranges of the Comptonized model parameters allowed by the observations. The count spectrum has a maximum at roughly 1 MeV, indicating that the spectral peak lies at that energy or above it, regardless of the details of spectral fitting. We substantiate this claim by fixing the photon index at the mean value for short GRBs, -0.42 for a model with an exponential cut-off above $E_{\text{pk}}^{\text{Comp}}$, and generate a distribution of amplitudes and peak energies for all the positions along the localization arc. We find that in 94.6% of the cases the peak energy exceeded 1 MeV indicating a high peak energy event similar to short GRBs (Figure 1, right). We also carry out a simulation where we fix the peak energy at 1 MeV and fit the amplitude and the photon index (Figure 1, left).

3. RADIATION FROM A STELLAR MASS BLACK HOLE MERGER

Significant EM energy release from a binary BH merger is unexpected. The dispersion length of grav-

¹ We note that while the cutoff energy could be constrained, the cutoff power law model is not statistically preferred over a power law spectrum.

itational waves is much larger than the curvature radius associated with material surrounding the merger in any conceivable scenario (e.g. Misner et al. 1973), thus no significant energy transfer is expected from GW to matter. Also, no obvious debris are expected from the BH-BH merger that can aid the energy release, similar to a BH-NS or NS-NS mergers (see however Loeb 2016; Murase et al. 2016; Perna et al. 2016; Yamazaki et al. 2016; Li et al. 2016).

In principle, a fraction $f_r(a) = 1 - \sqrt{(1 + \sqrt{1 - a^2})/2} \approx 6\%$ of the BH energy is available for extraction from a rotating BH. This corresponds to $E = 62f_r(0.67)M_\odot c^2 \approx 6.7 \times 10^{54}$ erg which is four orders of magnitude more than the observed energy release. Methods of tapping energy from the merged BH include neutrino driven disks (Zalamea & Beloborodov 2011), Blandford-Znajek (BZ) process (Blandford & Znajek 1977) (see however (Lyutikov 2016)).

More conventional models for energy release in a BH system can be put forward as follows: In the GW 150914 progenitor system about 5% of the initial total mass was radiated away as GW. Because of the reduced central mass, orbits of the fluid elements in a disk around the final BH will be modified (Bode & Phinney 2007), possibly producing shocks. Furthermore, the final BH will experience a kick associated with the anisotropic emission of GWs (Farris et al. 2011). The angular momentum vectors of the binaries were parallelized by interaction on long time scales with circumstellar matter implying the kick will launch the black hole into the surrounding disk with $v \lesssim 1000$ km s $^{-1}$, possibly enhancing the accretion rate. However, these mechanisms yield only $\lesssim L_E$ luminosities for conditions normally expected around BH mergers (e.g. Lippai et al. 2008).

3.1. Generic Blandford-Znajek scenario

We forgo pursuing the exact nature of energy release from the BH merger which later results in the electromagnetic counterpart. Specifically, we do not address the provenance of the disk material required to tap the energy of the BH. Given the unexpected association of the GW and EM signals, we outline the generic properties of a BH-disk system launching a jet with opening angle $\theta_{\text{jet}} = 0.1$ assuming the BZ mechanism. Our aim is to constrain the parameter space for this particular scenario through specific criteria.

We assume the disk height is $H(R) = R$, but for $H(R) \approx 0.3R$ as required by the model of Perna et al. (2016) the allowed parameter space does not change significantly. We illustrate the system parameters on a $R_{\text{disk}} - \dot{M}$ plane (see Figure 2). The disk has a viscosity parameter $\alpha_{\text{ST}} = 0.1$ (Shakura & Sunyaev 1973).

As a first criterion, we turn to the timescales governing

the launch of the putative jet. The accretion timescale, during which a jet of outer radius R_{out} is swallowed by a BH, can be calculated from the viscous timescale of the disk. As an example, for $R_{\text{out}} \sim 2 \times 10^8$ cm, the accretion time is $t_{\text{acc}} = (7/3\alpha)\sqrt{R_{\text{out}}^3/GM_{\text{BH}}} \approx 1 \alpha_{-1}^{-1}(R_{\text{out}}/2 \times 10^8 \text{ cm})^{3/2} (M_{\text{BH}}/62M_\odot)^{-1/2}$ s. The central engine timescale (the accretion timescale in our example, Zhang et al. (2009)) can be constrained to be at most the observed duration or $t_{\text{acc}} \lesssim 1$ s (Aloy et al. 2005). This constraint will carve out a region in Figure 2 to the left of the $t_{\text{acc}} = 1$ s or $R_{\text{out}} = 2.3 \times 10^8$ cm line.

Another criterion which can constrain the physical parameters of the system is the activation of the BZ mechanism. In order for the BZ mechanism to occur, the magnetohydrodynamic waves need to be able to escape the BH ergosphere (Komissarov & Barkov 2009). To first approximation, this translates to the Alfvén velocity, $v_A^2 \approx B^2/4\pi\rho$, being larger than the free-fall velocity, $v_{\text{ff}}^2 = 2GM_{\text{BH}}/R$. Here ρ is the disk density. Defining $\eta_{\text{BZ}} = v_A/v_{\text{ff}} = 4\pi\rho c^2/B^2$, for efficient energy extraction we require $\eta_{\text{BZ}} < 1$. The exact limit, depending on the rotation parameter, can be obtained by numerical simulations (Komissarov & Barkov 2009) and for $a = 0.7$ (see their Figure 3) it can go as low as $\eta_{\text{BZ}} < 0.3 - 0.5$. We conservatively take $\eta_{\text{BZ}} < 1$ at $R \approx R_H$, to result in a constraint of $R_{\text{out}} \gtrsim 7 \times 10^7$ cm (see Figure 2).

The accretion velocity (for adiabatic index $\hat{\gamma} = 4/3$) can be written as $v_{\text{in}} = (3\alpha/7)v_k$. The sound speed is $c_s^2 = (2/7)v_k^2$, where $v_k = \sqrt{GM_{\text{BH}}/R}$ is the Kepler velocity. Writing the mass accretion rate as, $\dot{M} = 2\pi R H \rho v_{\text{in}}$, we can express the pressure as $\hat{\gamma}P = \rho c_s^2$.

Assuming the magnetic field threading the BH at the marginally stable radius (R_0) is related to the thermal pressure through the magnetization parameter β , ($P = B^2\beta/(8\pi)$) according to Komissarov & Barkov (2010), we can write:

$$B \approx 5.4 \times 10^{11} \dot{M}_{-5}^{1/2} \left(\frac{f_1(a)}{2.48} \right)^{-5/4} \left(\frac{M_{\text{BH}}}{62M_\odot} \right)^{-1} \alpha_{-1}^{-1/2} \beta_1^{-1/2} \text{ G.} \quad (2)$$

where $f_1(a = 0.67) = 2.48$.

Next, we consider the BZ luminosity (L_{BZ}). We define $\Psi_h = 2\pi R_h^2 B_h$ as the magnetic flux threading the BH horizon, $\Omega_h = f_2(a)c^3/GM_{\text{BH}}$ is the angular velocity and $f_2(a) = a/(2 + 2\sqrt{1 - a^2})$. The expression for the BZ luminosity:

$$\begin{aligned} L_{\text{BZ}} &= \frac{1}{3c} \left(\frac{\Psi_h \Omega_h}{4\pi} \right)^2 \\ &= \frac{\sqrt{14} f_1^{3/2}(a) f_2^2(a)}{9\alpha\beta} \dot{M} c^2 \\ &= 1.1 \times 10^{48} \frac{\dot{M}_{-5}}{\alpha_{-1}\beta_1} \text{ erg s}^{-1}. \end{aligned} \quad (3)$$

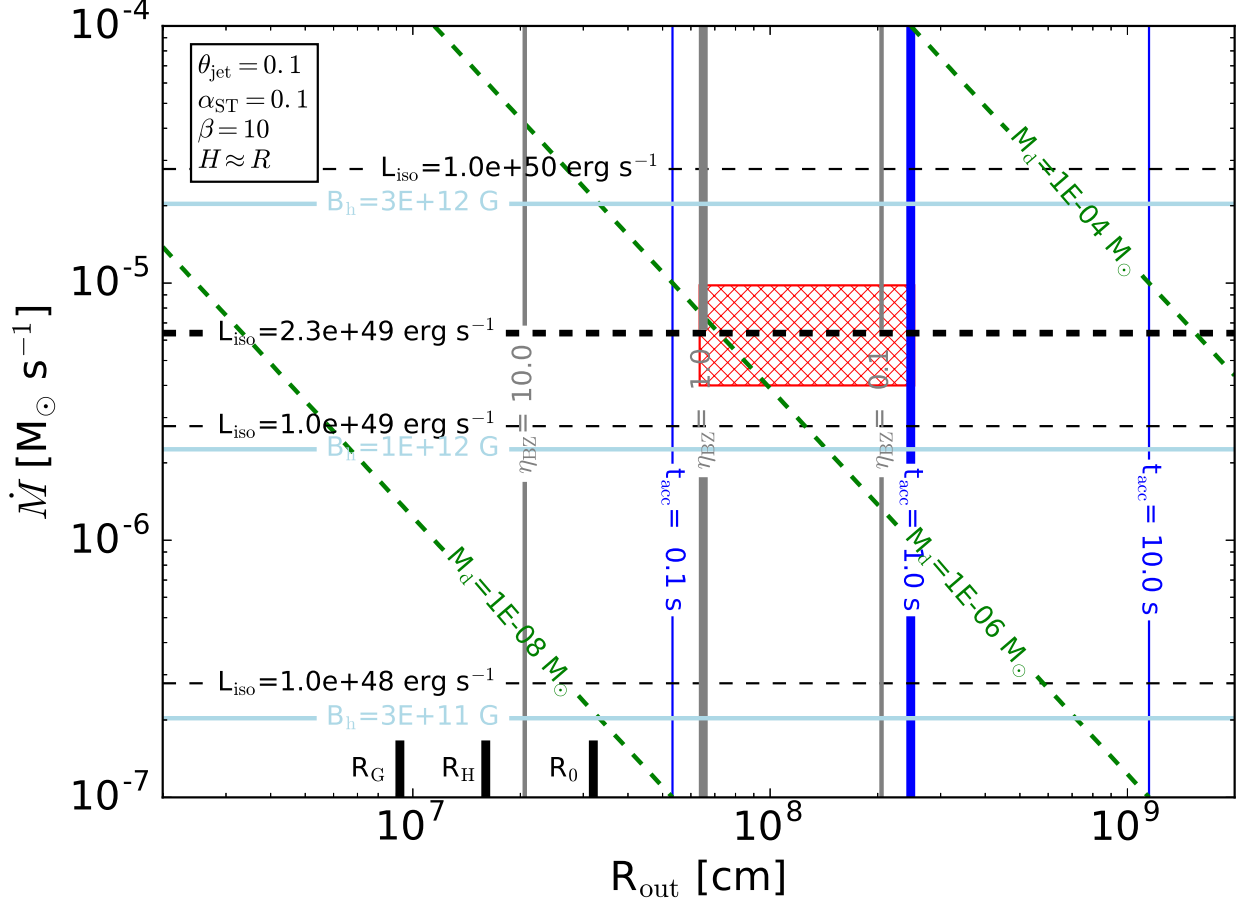


Figure 2. Disk parameter space constrained by the observations. The cross-hatched rectangle marks the approximate allowed outer disk radius and mass accretion rate. This is valid for an assumed jet opening angle of $\theta_{\text{jet}} = 0.1$. Isotropic equivalent (observed) luminosity is in black dashed lines, dark blue lines show the accretion timescale, light blue lines show the magnetic field strength, green dashed lines show the disk mass and gray lines show the BZ efficiency factor. On the bottom x axis we indicate the values of the gravitational radius, the horizon radius and the marginally stable (innermost stable) radius.

If the radiation emanates from a jet with half opening angle, θ_{jet} , the observed, isotropic equivalent luminosity is related to the BZ output power as $L_{\text{iso}} = L_{\text{BZ}} \theta_{\text{jet}}^{-2} / 2 = 200(\theta_{\text{jet}}/0.1)^{-2} L_{\text{BZ}}$. Thus, the observed isotropic equivalent luminosity can be expressed as a function of \dot{M} (assuming a jet opening angle) and it is possible to use it to constrain the allowed parameter space of \dot{M} (see L_{iso} lines on Figure 2). We draw the hatched region by allowing a factor of ~ 2 around the observed luminosity of $L_{\text{iso}} = 2.3 \times 10^{49} \text{ erg s}^{-1}$. In this scenario, we can constrain the disk mass to $10^{-6} - 10^{-5} M_\odot$, and the magnetic field threading the horizon will be $\sim 2 \times 10^{12} \text{ G}$.

4. RADIATION MECHANISMS

Focusing on the gamma-ray signal, it has both spectral and temporal properties consistent with the prompt emission of a short GRB. The observed luminosity is ~ 10 orders of magnitude larger than the Eddington luminosity, indicating gamma-ray source has likely expe-

rienced relativistic expansion. In the GRB fireball scenario the jet Lorentz factor is expected to go through the acceleration phase, starting from the launching radius (R_0), $\Gamma(R) = R/R_0$. When the accelerating material has kinetic energy per unit particle of $\sim \eta m_p c^2$ where $\eta = L/\dot{M}c^2 (\gtrsim 100 \text{ for GRBs})$ is the dimensionless entropy, we have $\Gamma \approx \eta = \text{constant}$. This point is marked by the saturation radius, $R_{\text{sat}} = R_0 \eta$. Starting at the deceleration radius (see Section 4.3), R_{dec} , the jet enters the self-similar deceleration phase, where $\Gamma(R) = \eta(R/R_{\text{dec}})^{-g}$, $3/2 < g < 3$ (Mészáros et al. 1993). Because of the weakness of the γ -ray source, we will only address peak energies of models and in some cases their fluence.

4.1. Photospheric models

In the relativistically expanding material the location where the Thompson scattering optical depth falls below unity marks the position of the photosphere. This is the

innermost radius from where radiation can escape and

$$R_{\text{phot}} \approx \begin{cases} 2.8 \times 10^7 \left(\frac{L}{L_{\text{obs}}} \right) \eta_3^{-3} \text{ cm} & \text{if } R_{\text{phot}} > R_{\text{sat}} \text{ or } \eta < \Gamma_T \\ 4.6 \times 10^9 \left(\frac{L}{L_{\text{obs}}} \right)^{1/3} \left(\frac{R_0}{R_*} \right)^{2/3} \eta_3^{-1/3} \text{ cm} & \text{if } R_{\text{phot}} < R_{\text{sat}} \text{ or } \eta > \Gamma_T, \end{cases} \quad (4)$$

where $\Gamma_T = 170 (L/L_{\text{obs}})^{1/4} (R_0/R_*)^{-1/4}$ is the Lorentz factor separating the photosphere in the acceleration phase ($\eta > \Gamma_T$) and the photosphere in the coasting phase ($\eta < \Gamma_T$). We note here that based on the joint GW and EM observations this quantity can be well determined. Henceforth, for brevity we use $L_{\text{obs}} = 2.3 \times 10^{49} \text{ erg s}^{-1}$ and $R_* = 3.2 \times 10^7 \text{ cm}$ to mark the numerical scaling values for the observed luminosity and the calculated launching radius respectively. $R_{\text{sat}} = R_0 \Gamma \approx 3.2 \times 10^{10} (R_0/R_*) \Gamma_3 \text{ cm}$. The fact that the actual Lorentz factor, $\Gamma \gtrsim 1000$ is likely larger than Γ_T (see e.g. Section 4.3) suggests the photosphere occurs in the acceleration region. E.g. for $\Gamma = 10^3$, we have $R_{\text{phot}} \approx 3 \times 10^9 \text{ cm} < R_{\text{sat}}$. The observed temperature of an expanding fireball at its photosphere (occurring in the acceleration phase) can be calculated as $T_0 \approx (L/4\pi R_0^2 c a)^{1/4} \approx 1 (L/L_{\text{obs}})^{1/4} (R_0/R_*)^{-1/2} \text{ MeV}$. The maximum attainable peak energy of a spectrum with temperature T (Li & Sari 2008; Fan et al. 2012; Zhang et al. 2012):

$$E_{\text{pk}}^{\text{PH}} \lesssim 3.92 \times kT_0 \approx 0.6 \left(\frac{L}{L_{\text{obs}}} \right)^{1/4} \left(\frac{R_0}{R_*} \right)^{-1/2} \text{ MeV}. \quad (5)$$

The 3.92 factor indicates that the E_{pk} is the peak in the νF_ν representation. The fact that we know R_* , the smallest possible launching radius from the GW observations, we know Equation 5 is a strict upper limit for the temperature of the non-dissipative photosphere. The measured peak can reach the upper limit in Equation 5 in the case where the photosphere occurs in the acceleration region. In this case the comoving temperature is proportional to R^{-1} and the increase of the Lorentz factor ($\propto R$) compensates the decrease to yield a temperature of T_0 .

The peak energies of the simulated set of Comptonized spectra violate this limit (see Figure 1, right) in an overwhelming number of cases. Thus, even with the uncertainties of the spectral parameters, we consider this model is not favored by the data, however we cannot rule it out.

A more sophisticated class of models for the GRB prompt emission are *dissipative* photosphere models (Rees & Mészáros 2005). In these models energy is liberated while the flow is still optically thick through e.g. neutron-proton collisions (Beloborodov 2010) or mag-

netic reconnection (Giannios & Spruit 2007). There are no simple criteria for meaningful comparisons with data for GW 150914-GBM. For these models, in general terms, the peak energy is not constrained by the expression in Equation 5 and can reach substantially higher values $\lesssim 20 \text{ MeV}$ (Beloborodov 2013). E.g. for the observed luminosity of $2.3 \times 10^{49} \text{ erg s}^{-1}$, the maximum achievable peak energy is around $\sim 10 \text{ MeV}$ both for magnetic field dominated outflows and for baryon dominated cases as well (see Figure 2 of Veres et al. 2012).

4.2. Internal shocks

Internal shocks can occur in unsteady relativistic outflows (Rees & Mészáros 1994) where a faster shell catches up with a slower one. The colliding shells produce shocks that accelerate electrons, amplify the magnetic field and in turn the electrons emit synchrotron radiation. This process can tap the relative kinetic energy of material ejected at different times from the central object.

The radius of internal shocks can be calculated as $R_{\text{IS}} \approx 2c\Gamma^2 dt$, where dt is the variability timescale. For short GRBs, the average dt is $\approx 10^{-2} \text{ s}$ (MacLachlan et al. 2013). The detailed temporal structure of the gamma-ray lightcurve could not be determined by the GBM data for this weak event. Based on the GW observations, however, we can put a lower limit on the variability timescale that is the dynamic time $t_{\text{dyn}} = R_0/c = 1.1 \times 10^{-3} R_0/R_* \text{ s}$ such that $dt \gtrsim t_{\text{dyn}}$. The internal shock radius (R_{IS}) will be well above the photosphere, implying an optically thin outflow.

The synchrotron peak frequency will be at $E_{\text{peak}} = hq_e/(2\pi m_e c) \Gamma \gamma_e^2 B$. For $\gamma_e = (m_p/2m_e)\epsilon_e \approx 940 \epsilon_e$ and $B = \sqrt{2\epsilon_B L T_\gamma / (\Gamma^2 c dt)^3} = 4 \times 10^7 (L/L_{\text{obs}})^{1/2} \epsilon_B^{-3/2} T_{\gamma,0}^{1/2} \text{ G}$ (Panaitescu & Mészáros 2000), the peak will be at:

$$E_{\text{pk}}^{\text{IS}} \lesssim 0.54 (L/L_{\text{obs}})^{1/2} \Gamma_3^{-1} dt_{-3}^{-3/2} \epsilon_B^{1/2} \epsilon_e^2 T_\gamma^{1/2} \text{ MeV}. \quad (6)$$

A more thorough analysis considering pairs and the width of the shells (Guetta et al. 2001) yields a stricter limit:

$$E_{\text{pk}}^{\text{IS}} \lesssim 80 (L/L_{\text{obs}})^{1/6} (\Delta/R_0)^{-5/6} dt_{-3}^{1/6} \epsilon_B^{1/2} \epsilon_e^{4/3} \text{ keV}. \quad (7)$$

Here, Δ is the width of the shell which has to be greater than R_0 . Note that here, the electron and magnetic field

equipartition parameters ϵ_e and ϵ_B are normalized to 1.

With the spectral peak constrained to be reliably above 1 MeV, the above derivation suggests the internal shock model has difficulties in accounting for peak energies above 0.5 MeV with a given launching radius. Keeping in mind the large errors on the observed quantities, we can say this model does not naturally explain the observed peak energy, however, just as in the case of the non-dissipative photosphere models, we cannot completely rule it out.

4.3. External shocks

External shocks were initially proposed (Rees & Meszaros 1992) as a model for GRB prompt emission, but had problems interpreting the strong variability of lightcurves (Kobayashi et al. 1997) (see however Dermer & Mitman (1999)). On the other hand is a very successful model for interpreting the multiwavelength afterglow (Mészáros & Rees 1997; Chiang & Dermer 1999). Recently however, claims of external shock origin for the prompt emission have been reported for bursts with smooth, simple lightcurves (Burgess et al. 2016). External shocks are almost guaranteed to form around a relativistically expanding shell. Here we apply the formalism of the external shock model to constrain the physics of the GW associated GW 150914-GBM event.

A shock front develops as the material from the central engine interacts with the interstellar material (ISM). The timescale on which this occurs is the deceleration time. It marks the time where the material plowed up by the relativistic jet corresponds roughly $1/\Gamma$ times the mass in the ejecta. For interstellar material of number density n , Lorentz factor Γ , and kinetic energy E_k we have

$$t_{\text{dec}} \approx 0.28 n_{-3}^{-1/3} \Gamma_3^{-8/3} (E/E_k)^{1/3} \text{ s}. \quad (8)$$

Based on Zhang et al. (2007)'s results for short GRBs, we assume a radiative efficiency $\eta_\gamma = E_{\text{ph}}/(E_k + E_{\text{ph}}) = 0.5$ and get $E_k \approx E_{\text{ph}} \approx L_{\text{obs}} \times 1 \text{ s} \approx 2.3 \times 10^{49} \text{ erg}$.

The peak flux density of the spectrum can be calculated by adding the individual electron powers and according to (Sari et al. 1998; Gao et al. 2013):

$$F_{\nu, \text{p}} = \frac{N_e P_{\nu, \text{max}}}{4\pi D_L^2}, \quad (9)$$

where $P_{\nu, \text{max}} = m_e c^2 \sigma_T \Gamma B / 3q_e$ is the single electron synchrotron power, $N_e = 4\pi R_{\text{dec}}^3 n / 3$ is the number of swept up electrons, $R_{\text{dec}} \approx 2\Gamma^2 c t_{\text{dec}}$ is the deceleration radius and $B = \sqrt{32\pi\epsilon_B n m_p c^2 \Gamma^2}$ is the magnetic field in the shocked region. ϵ_e and ϵ_B are the electron and magnetic field equipartition parameters respectively.

The peak energy, corresponding to electron random

Lorentz factor of $\gamma \approx 600\epsilon_e \Gamma$ is

$$E_{\text{pk}}^{\text{ES}} = \frac{q_e B \gamma^2 \Gamma}{2\pi m_e c} = 1.1 \left(\frac{\Gamma}{2000} \right)^4 n_{-3}^{1/2} \left(\frac{\epsilon_e}{0.5} \right)^2 \left(\frac{\epsilon_B}{0.5} \right)^{1/2} \text{ MeV}. \quad (10)$$

The peak of the external shock radiation occurs approximately at the deceleration time. We know the delay of the EM trigger compared to the GW signal, and we require $t_{\text{dec}} \lesssim \Delta t_{\gamma\text{-GW}}$. We draw the deceleration time values on Figure 3 with light blue, and note that our Monte Carlo simulated spectral parameters overwhelmingly result in a deceleration time lower than the $\Delta t_{\gamma\text{-GW}}$.

We use the measurement of the peak energy (the fact that it is likely above 1 MeV) and the peak flux density from the Comptonized spectrum in the case for the fixed photon index (Figure 1, right) to place constraints on the particle number density around the progenitor and the Lorentz factor of the outflow. On Figure 3 we show that the two constraints mark a region centered around $n \approx 6 \times 10^{-4} \text{ cm}^{-3}$ and $\Gamma \approx 2300$. The shaded region on Figure 3 shows a two dimensional histogram of simulated values (darker shades mark more cases within the region) pointing out the non-trivial shape of the uncertainties on Γ and n . The peak flux lines (red) are the median and the values corresponding to the full width at half maximum of the $F_{\nu, \text{p}}$ distribution. The corresponding magnetic field strength is $B \approx 20 \text{ G}$, the radius of peak emission is $R_{\text{dec}} \approx 10^{16} \text{ cm}$ and the deceleration time is $t_{\text{dec}} \approx 4 \times 10^{-2} \text{ s}$. With these parameters the synchrotron radiating electrons are in the fast cooling regime, which means they lose their energy faster than the dynamical timescale and this is in line with expectations for the prompt emission. This exercise can be carried out with a wind profile interstellar medium, but for compact mergers the constant density profile is preferred (e.g. Panaitescu et al. 2006).

We note here that in the external shock scenario in its simplest, impulsive energy injection case, the timescale of the GRB duration is also governed by the deceleration time. However, since the derived t_{dec} ($4 \times 10^{-2} \text{ s}$) and the GRB duration ($T_{\text{GRB}} \approx 1 \text{ s}$) differ, we argue that the GRB duration reflects the energy injection timescale, which can be of the order of 1 s, instead of t_{dec} .

We set the microphysical parameters (ϵ_e , ϵ_B) to 0.5. Although we are using this model to constrain the prompt emission, based on afterglow modeling these parameters would in general have lower values. E.g. typical afterglow-based values would be $\epsilon_e = 0.1$ and $\epsilon_B = 10^{-2}$. The decrease in the microphysical parameters would have to be compensated by an increase of the Lorentz factor and ISM density (to have the same peak energy and flux) which would result in $\Gamma \sim 5300$ and $n \sim 2.2 \times 10^{-2} \text{ cm}^{-3}$.

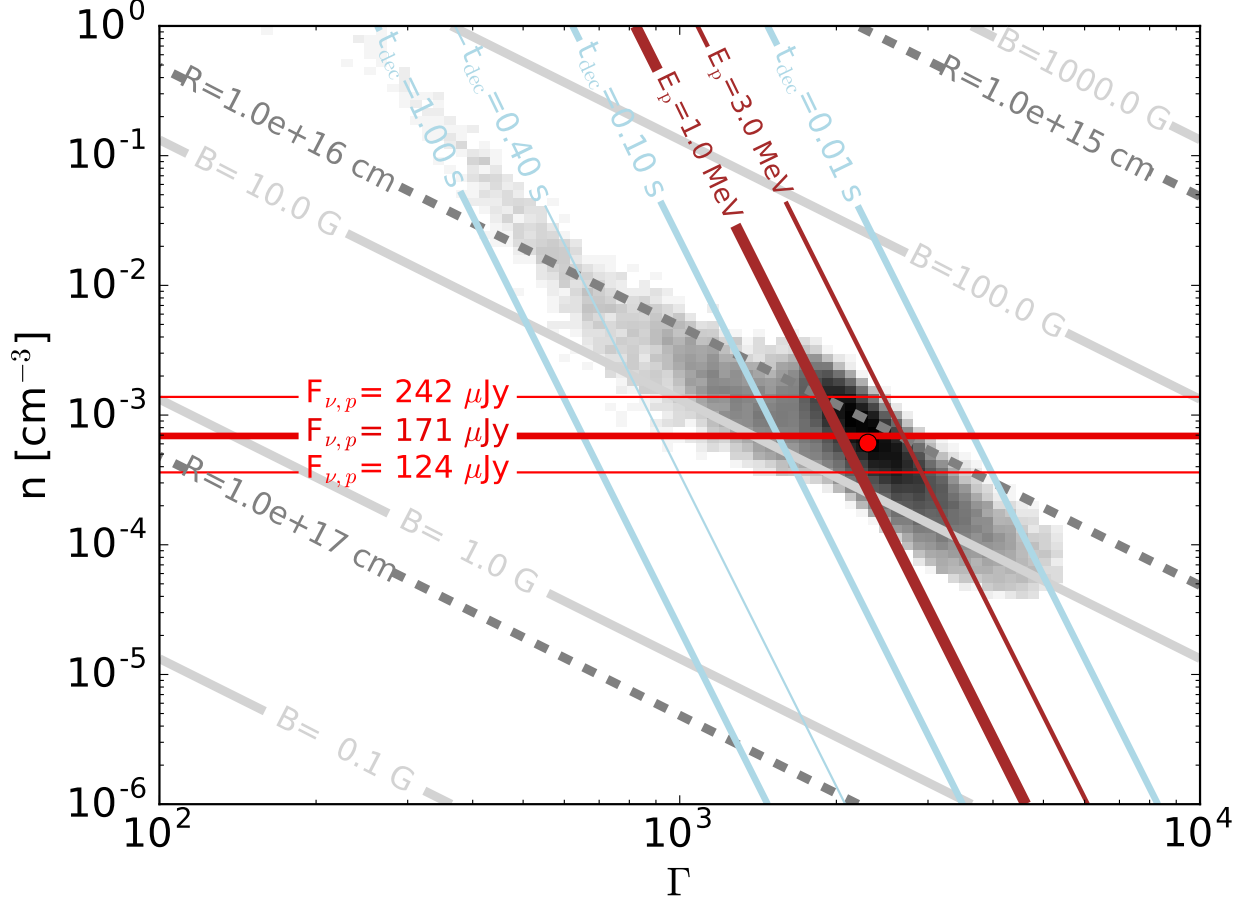


Figure 3. Lorentz factor- ISM density plane with constraints plotted for the external shock scenario. Here, the photon index in the Comptonized model is fixed to -0.42 . Different colors and styles mark different physical quantities, all displayed on the contour lines. The intersecting regions of brown and red contour lines (E_{peak} and $F_{\nu, \text{peak}}$) mark the favored parameter space (the red circle is at $n = 8 \times 10^{-4} \text{ cm}^{-3}$ and $\Gamma = 2300$). The underlying histogram shows the results of a Monte Carlo simulation for the allowable spectral parameters. Darker bins indicate more cases. We have assumed $\epsilon_e = \epsilon_B = 0.5$.

4.3.1. Efficiency of external shocks

The above results were presented for an efficiency of 0.5 ($E_k = E_{\text{ph}}$). In the external shock scenario, the radiation taps the kinetic energy of the explosion. Higher than 50% radiative efficiency is unexpected for external shocks. [Dermer & Mitman \(1999\)](#), for example, find that 10% ($E_k = 9E_{\text{ph}}$) efficiency is more consistent with this scenario. In this case, the measured fluence and the peak energy yields a Lorentz factor and external density of $(4 \times 10^{-5} \text{ cm}^{-3}, 3300)$. These are even more extreme than the values for 50% efficiency, but consistently point to the low density origin of the binary source. The deceleration time is somewhat larger in this case, $t_{\text{dec}} \approx 8 \times 10^{-2} \text{ s}$, but still within the $t_{\text{GRB}} - t_{\text{GW}} = 0.4 \text{ s}$.

4.3.2. External shock model with an average short GRB

Because the peak energy is difficult to constrain for this event we analyze another possible scenario. We

take the *average* photon index and peak energy for a Comptonized spectrum of the short GRB sample for GBM ([Gruber et al. 2014](#))². We fit the spectral data and generate amplitude parameters (A in Equation 1) for the Comptonized spectrum by fixing $\alpha_{\text{short}} = -0.42$, $E_{\text{pk, short}}^{\text{Comp}} = 566 \text{ keV}$ and using response matrices generated for the 11 positions along the Advanced LIGO localization arc. We get a distribution of peak fluxes for the fixed value of the peak energy. It is possible then to put these parameters to the Lorentz factor density plane (see Figure 4) and deduce that the required density distribution peaks around $5 \times 10^{-4} \text{ cm}^{-3}$ with a tail extending to a few $\times 10^{-3} \text{ cm}^{-3}$ and the Lorentz factor is $\Gamma \approx 1800$. The deceleration time for this case is $\approx 0.1 \text{ s}$, which is again consistently lower than the 0.4 s delay

² The up-to-date catalog is located at: <http://heasarc.gsfc.nasa.gov/W3Browse/fermi/fermigbrst.html>

between the GW and EM signal.

5. DISCUSSION AND CONCLUSION

Assuming the binary black hole merger is associated with the gamma-ray signal detected by GBM, we have taken the leading prompt emission models for GRBs and applied it to the observations of GW 150914-GBM, aided by the accurately determined central engine parameters through GW measurements. We find that the non-dissipative photosphere and the internal shock models have some difficulty in interpreting the observations, though at this point no model can be definitely ruled out, while a dissipative photosphere model is unconstrained. The external shock model is able to interpret both the high peak energy and the observed flux yielding constraints on the Lorentz factor of the explosion ($\gtrsim 1000$) and the interstellar density ($\sim 10^{-3} \text{ cm}^{-3}$). The lower than usual ISM density is in line with the expectation that the merger takes place far from the birthplaces of its components (e.g. in a galactic halo environment). Furthermore, the low density might be a more general property of the external shock model itself which, applied to model afterglow observations of GRBs with $\gtrsim \text{GeV}$ photons (e.g. GRB 090510A) yield similarly high Γ and low n (De Pasquale et al. 2010). If we assume spectral parameters characteristic of short GRBs, we still consistently find high Γ and low n .

Even though our results are not definitive, the strength of such an approach lies in constraining values of the launching radius through GW observations and address EM observations.

Further GW observations with better coverage from GBM will settle if merging BH binaries indeed emit γ -rays. It is possible however, that due to observer angle effects, the GRB-GW association will only be settled

once a sizeable sample of GW and gamma-ray observations has accumulated. Indeed, GW signals from compact mergers are not strongly dependent on the orientation of the binary while prompt gamma-rays are essentially not expected if we are not inside the jet opening angle. On the other hand, edge-on systems have on average $1/\sqrt{8}$ the signal of the face-on cases. This results in an increased likelihood that the systems detected by Advanced LIGO are face-on than edge-on. By measuring the jet opening angle for a GRB, we can constrain the available parameter space for the inclination, measured by the Advanced LIGO. Furthermore, detailed multi-wavelength afterglow modeling (e.g. Zhang et al. 2015) can also constrain the viewing angle.

Once GW observations become routine, and their EM counterparts will be readily available, we will be able to address the question of the association of short GRBs with BH mergers on a more solid footing. As an example of investigating GW 150914-GBM as a member of the short GRB population, Li et al. (2016) argued that it is an outlier on the $E_{\text{pk}} - L_{\text{iso}}$ diagram for short GRBs. This may indicate a different progenitor for the GBM event. However, due to a small sample size, the correlation for previous short GRBs is not strong enough for a definite conclusion.

With our current understanding of GRBs, variability timescale of the GRB lightcurve can provide a limit on the size of the jet launch. If the GW-GRB association is confirmed, the variability times can be compared to the marginally stable radii resulting from the GW detection. Thus it will be possible to rule out some classes of models more firmly with similar analysis to the one presented here.

Acknowledgements - We thank Tyson Littenberg and Michael Briggs for discussions. This study was supported by Fermi grant NNM11AA01A. P.M. acknowledges support from NASA NNX13AH50G.

REFERENCES

- Abbott, B. P., Abbott, R., Abbott, T. D., et al. 2016a, Physical Review Letters, 116, 061102
- . 2016b, Physical Review Letters, 116, 241102
- Aloy, M. A., Janka, H.-T., & Müller, E. 2005, A&A, 436, 273
- Beloborodov, A. M. 2010, MNRAS, 407, 1033
- . 2013, ApJ, 764, 157
- Blandford, R. D., & Znajek, R. L. 1977, MNRAS, 179, 433
- Bode, N., & Phinney, S. 2007, in APS April Meeting Abstracts
- Burgess, J. M., Bégué, D., Ryde, F., et al. 2016, ApJ, 822, 63
- Chiang, J., & Dermer, C. D. 1999, ApJ, 512, 699
- Connaughton, V., Briggs, M. S., Goldstein, A., et al. 2015, ApJS, 216, 32
- Connaughton, V., Burns, E., Goldstein, A., et al. 2016, ApJL, 826, L6
- Corsi, A., & Mészáros, P. 2009, ApJ, 702, 1171
- Cutler, C., & Flanagan, É. E. 1994, PhRvD, 49, 2658
- De Pasquale, M., Schady, P., Kuin, N. P. M., et al. 2010, ApJL, 709, L146
- Dermer, C. D., & Mitman, K. E. 1999, ApJL, 513, L5
- Eichler, D., Livio, M., Piran, T., & Schramm, D. N. 1989, Nature, 340, 126
- Fan, Y.-Z., Wei, D.-M., Zhang, F.-W., & Zhang, B.-B. 2012, ApJL, 755, L6
- Farris, B. D., Liu, Y. T., & Shapiro, S. L. 2011, PhRvD, 84, 024024
- Fraschetti, F. 2016, ArXiv e-prints, arXiv:1603.01950
- Gao, H., Lei, W.-H., Zou, Y.-C., Wu, X.-F., & Zhang, B. 2013, New Astronomy Review, 57, 141
- Giannios, D., & Spruit, H. C. 2007, A&A, 469, 1
- Gruber, D., Goldstein, A., Weller von Ahlefeld, V., et al. 2014, ApJS, 211, 12
- Guetta, D., Spada, M., & Waxman, E. 2001, ApJ, 557, 399
- Kobayashi, S., & Mészáros, P. 2003, ApJ, 589, 861

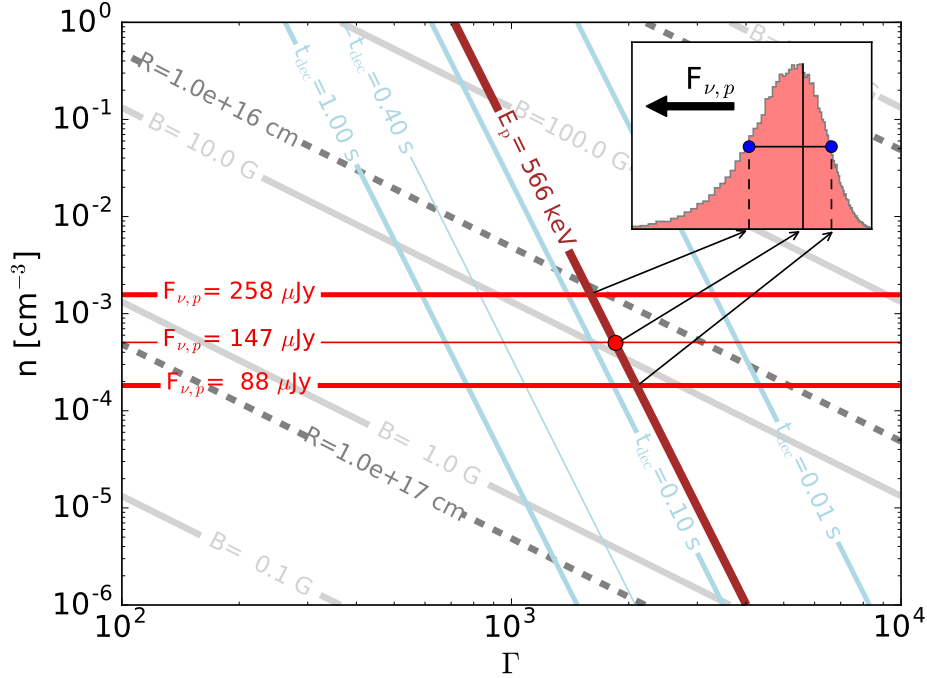


Figure 4. Lorentz factor- ISM density plane with the peak energy fixed to the average value for short GRBs, and peak flux results from spectral fitting. The contours are marked similar to Figure 3 with the physical quantities indicated on the contour lines. The inset shows the peak flux distribution with the thin arrows indicating the median value and the errors in the distribution. The thick arrow indicates $F_{\nu,p}$ values increase to the left. The red circle marks the most likely set of parameters, $n = 5 \times 10^{-4} \text{ cm}^{-3}$ and $\Gamma = 1800$. As before, we have assumed $\epsilon_e = \epsilon_B = 0.5$.

- Kobayashi, S., Piran, T., & Sari, R. 1997, *ApJ*, 490, 92
 Komissarov, S. S., & Barkov, M. V. 2009, *MNRAS*, 397, 1153
 —. 2010, *MNRAS*, 402, L25
 Kumar, P., & Zhang, B. 2015, *PhR*, 561, 1
 Larsson, J., Racusin, J. L., & Burgess, J. M. 2015, *ApJL*, 800, L34
 Li, C., & Sari, R. 2008, *ApJ*, 677, 425
 Li, X., Zhang, F.-W., Yuan, Q., et al. 2016, *ArXiv e-prints*, arXiv:1602.04460
 Lippai, Z., Frei, Z., & Haiman, Z. 2008, *ApJL*, 676, L5
 Loeb, A. 2016, *ApJL*, 819, L21
 Lyutikov, M. 2016, *ArXiv e-prints*, arXiv:1602.07352
 MacLachlan, G. A., Shenoy, A., Sonbas, E., et al. 2013, *MNRAS*, 432, 857
 Mészáros, P., Laguna, P., & Rees, M. J. 1993, *ApJ*, 415, 181
 Mészáros, P., & Rees, M. J. 1997, *ApJ*, 476, 232
 Meszaros, P., & Rees, M. J. 2014, *ArXiv e-prints*, arXiv:1401.3012
 Misner, C. W., Thorne, K. S., & Wheeler, J. A. 1973, *Gravitation*
 Murase, K., Kashiyama, K., Mészáros, P., Shoemaker, I., & Senno, N. 2016, *ApJL*, 822, L9
 Nalewajko, K. 2012, *MNRAS*, 420, L48
 Paczyński, B. 1986, *ApJL*, 308, L43
 Panaitescu, A., & Mészáros, P. 2000, *ApJL*, 544, L17
 Panaitescu, A., Mészáros, P., Burrows, D., et al. 2006, *MNRAS*, 369, 2059
 Pe’er, A., Ryde, F., Wijers, R. A. M. J., Mészáros, P., & Rees, M. J. 2007, *ApJL*, 664, L1
 Perna, R., Lazzati, D., & Giacomazzo, B. 2016, *ApJL*, 821, L18
 Rees, M. J., & Meszaros, P. 1992, *M.N.R.A.S.*, 258, 41P
 Rees, M. J., & Mészáros, P. 1994, *ApJL*, 430, L93
 Rees, M. J., & Mészáros, P. 2005, *ApJ*, 628, 847
 Sari, R., Piran, T., & Narayan, R. 1998, *ApJL*, 497, L17+
 Savchenko, V., Ferrigno, C., Mereghetti, S., et al. 2016, *ApJL*, 820, L36
 Shakura, N. I., & Sunyaev, R. A. 1973, *A&A*, 24, 337
 Veres, P., Zhang, B.-B., & Mészáros, P. 2012, *ApJL*, 761, L18
 Yamazaki, R., Asano, K., & Ohira, Y. 2016, *Progress of Theoretical and Experimental Physics*, 2016, 051E01
 Zalamea, I., & Beloborodov, A. M. 2011, *MNRAS*, 410, 2302
 Zhang, B. 2016, *ArXiv e-prints*, arXiv:1602.04542
 Zhang, B., Lu, R.-J., Liang, E.-W., & Wu, X.-F. 2012, *ApJL*, 758, L34
 Zhang, B., Liang, E., Page, K. L., et al. 2007, *ApJ*, 655, 989
 Zhang, B., Zhang, B.-B., Virgili, F. J., et al. 2009, *ApJ*, 703, 1696
 Zhang, B.-B., van Eerten, H., Burrows, D. N., et al. 2015, *ApJ*, 806, 15